Chinese Chemical Letters 34 (2023) 107121

Contents lists available at ScienceDirect

Chinese Chemical Letters

journal homepage: www.elsevier.com/locate/cclet

Synthesis and application of single-atom catalysts in sulfur cathode for high-performance lithium–sulfur batteries

Yingjie Miao[a], Yufan Zheng[b], Feng Tao[a], Zhijun Chen[c], Yi Xiong[a], Fengzhang Ren[a,*], Yong Liu[a,*]

[a] Provincial and Ministerial Co-Construction of Collaborative Innovation Center for Non-Ferrous Metal New Materials and Advanced Processing Technology, Henan Key Laboratory of Non-Ferrous Materials Science and Processing Technology, School of Materials Science and Engineering, Henan University of Science and Technology, Luoyang 471023, China
[b] School of Intelligent Manufacturing Ecosystem, Xi'an Jiaotong – Liverpool University, Suzhou 215123, China
[c] Luoyang Bearing Research Institute Co., Ltd., Luoyang 471039, China

ARTICLE INFO

Article history:
Received 3 December 2021
Revised 27 December 2021
Accepted 6 January 2022
Available online 13 January 2022

Keywords:
Single-atom catalysts
Lithium–sulfur batteries
Sulfur cathode
Synthesis and application
Polysulfide conversion
Shuttle effect

ABSTRACT

Lithium–sulfur (Li-S) batteries are regarded as one of the most promising energy storage devices because of their low cost, high energy density, and environmental friendliness. However, Li-S batteries suffer from sluggish reaction kinetics and serious "shuttle effect" of lithium polysulfides (LiPSs), which causes rapid decay of battery capacity and prevent their practical application. To address these problems, introducing single-atom catalysts (SACs) is an effective method to improve the electrochemical performance of Li-S batteries, due to their high catalytic efficiency and definite active sites for LiPSs. In this paper, we summarized the latest developments in enhancing the electrochemical performance of cathode for Li-S batteries through introducing different SACs. Furthermore, we briefly introduced the catalytic mechanism of SACs and discussed the strategies of synthesizing SACs, including the spatial confinement strategy and the coordination design strategy. Finally, the challenges and prospects in this field are proposed. We believe that this review would help to design and fabricate high-performance Li-S batteries *via* introducing SACs and boost their practical application.

1. Introduction

Nowadays, the overcomsumption of limited traditional fossil fuels causes severe environmental pollution and energy crisis, so it is urgent for us to look for clean and renewable energy sources, such as wind energy, solar energy, water energy [1,2]. However, these energy sources are intermittent and cannot provide stable energy output. This requires an advanced energy storage system, which limits its application [3,4]. Fortunately, the electrochemical energy storage system has become a promising solution due to its outstanding electrochemical energy storage and release capabilities [5,6]. In addition, lithium ion batteries have been widely used in energy storage system, because of their low self-discharge rate and other advantages [7–10]. However, because of the limited energy density (140–260 Wh/kg), they can no longer meet the ever-increasing demands of large-scale energy storage, so we need to develop a new generation of energy storage batteries [11–13]. Because of the advantages of eco-friendly and high theoretical energy density (2500 Wh/kg), lithium–sulfur (Li-S) batteries have been acknowledged as the most promising battery systems for energy storage [14–16]. However, Li-S batteries also have some problems during the charging and discharging process. For example, soluble lithium polysulfides (LiPSs) (Li_2S_n, $4 \leq n \leq 8$) are formed during charge and discharge, which shuttle back and forth between the cathode and anode as the reaction progresses [17,18]. This serious shuttle effect reduces the utilization of sulfur. At the same time, due to the poor conductivity of S and Li_2S_2/Li_2S, higher energy is required for the reaction, which results in sluggish reaction kinetics [19–23]. And this also limits the actual energy density of Li-S batteries. Recently, introducing catalytic materials into Li-S batteries have been considered as an efficient strategy to enhance the reaction kinetics of batteries and alleviate the shuttle effect.

In recent years, several polar materials have been extensively studied regarding their chemisorption and catalytic sites. For instance metal oxides [24], sulfides [25], nitrides [26], carbides [27], phosphides [28] and their composite materials. These polar materials can not only possess strong absorption toward LiPSs, but also catalyze the conversion of LiPSs to Li_2S_2/Li_2S, which help to reduce

* Corresponding authors.
E-mail addresses: renfz@haust.edu.cn (F. Ren), liuyong209@haust.edu.cn (Y. Liu).

https://doi.org/10.1016/j.cclet.2022.01.014
1001-8417/

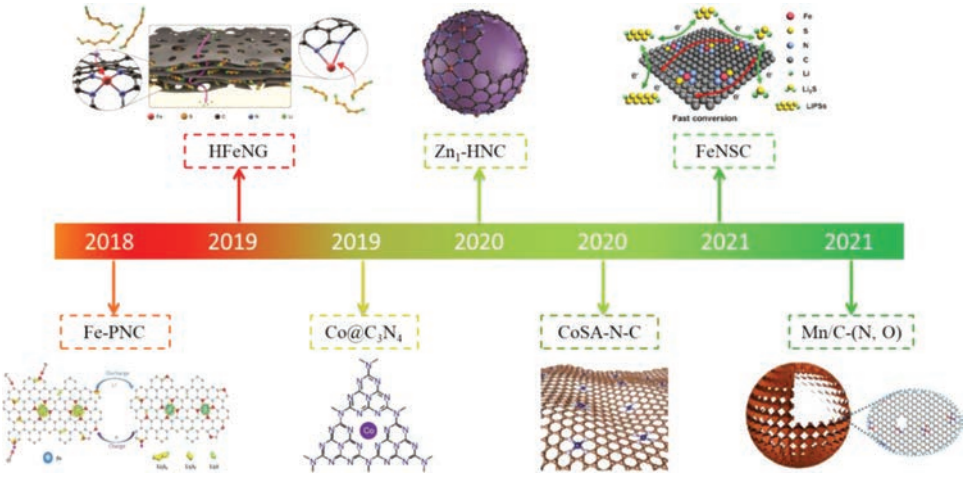

Fig. 1. Timeline of major representative examples of single-atom catalysts (SACs) for lithium-sulfur (Li-S) batteries cathode applications. The image for single iron-and nitrogen-doped carbon (Fe-PNC) is adapted with permission [38]. Copyright 2018, American Chemical Society. The image for the holey Fe, N codoped graphene (HFeNG) is adapted with permission [70]. Copyright 2019, Wiley-VCH. The image for cobalt atoms dispersed on hierarchical carbon nitride ($Co@C_3N_4$) is adapted with permission [68]. Copyright 2019, Elsevier B.V. The image for single atom Zn-decorated hollow carbon spheres (Zn_1–HNC) is adapted with permission [81]. Copyright 2020, Wiley-VCH. The image for SACs Co on nitrogen-doped carbon nanosheet (CoSA-N-C) is adapted with permission [63]. Copyright 2020, Elsevier B.V. The image for single-atom iron on nitrogen- and sulfur-doped porous carbon (FeNSC) is adapted with permission [21]. Copyright 2021, American Chemical Society. The image for single manganese (Mn) atoms implanted in oxygen and nitrogen double-doped hollow carbon sphere frameworks (Mn/C-(N, O) is adapted with permission [85]. Copyright 2021, Elsevier B.V.

the shuttle effect and increase the electrochemical kinetics [29]. Nevertheless, these strategies generally require a large number of catalysts. This will not only decrease the surface area of the host and lead to low sulfur loading, but also reduce the electronic conductivity which subtracts the utilization of sulfur [30]. Moreover, because these catalytic materials usually have a relatively complex structure and composition, their catalytic sites are often unclear and the reaction mechanism is difficult to explain [31]. Therefore, there is an urgent need to explore catalysts with outstanding electrical conductivity and well-defined active centers so as to achieve the practical application potential of Li-S batteries. In recent years, single atom catalysts (SACs) have attracted widespread attention for their excellent catalytic performance and maximum atomic utilization efficiency [32,33]. In addition, compared with other catalytic materials, SACs have a clear active center, which is convenient to illuminate the relationship between their structure, catalytic activity and the deep catalytic mechanism at the molecular level [34,35]. At present, the exploration of the application of SACs in Li-S batteries is still in the initial stage, so people have made a lot of efforts to this end. Researchers have found that SACs can catalyze the rapid conversion of LiPSs, reduce the shuttle effect, increase the actual capacity of Li-S batteries and greatly facilitate the development of high-performance Li-S batteries [36,37]. For example, Liu *et al.* composited single-atoms (SAs) iron with porous nitrogen-doped carbon (PNC) materials to obtain Fe-PNC and used it in the cathode of Li-S batteries. Due to the introduction of SAs Fe, the reversible conversion of S and Li_2S_2/Li_2S during the charging and discharging process is greatly improved [38]. Furthermore, Du *et al.* prepared SAs Co embedded in nitrogen-doped graphene (Co/NG) composite materials. The results showed that SAs Co coordinated with N and C acted as the active center of the dual-functional catalyst, which promoted the formation and decomposition of Li_2S during discharge and charging, respectively [39]. In addition to experimental articles, some recent advances in SACs for Li-S batteries have also been reviewed. For instance, Wang *et al.* reviewed recent progress in SACs for Li-S batteries. They highlighted the application of SACs in the cathodes, separators, interlayers, electrolytes, and anodes [40]. Moreover, Xiao *et al.* summarized the synthesis, characterization and electrochemical performance of SACs in metal sulfur batteries [41]. However, to the best of our knowledge, comprehensive reports on the synthesis strategies and applications of SACs in Li-S batteries, especially in the field of the cathode, are rarely reported.

Here, we summarize the recent progress of SACs in Li-S batteries. Fig. 1 provides representative examples of SACs used in the cathode of Li-S batteries in recent years, showing that researchers are making continuous efforts in this area. In addition, more and more different types of SACs have been developed and used in Li-S battery cathode materials. So first, we review the strategies of synthesizing SACs in Li-S batteries cathodes, including the spatial confinement strategy and the coordination design strategy. Moreover, the application of different kinds of SACs in the cathode of Li-S batteries, such as iron, cobalt and zinc, are described in expatiate. Finally, we discuss the challenges and prospects in this area. Hopefully, this review will stimulate more interest in SACs research, develop more SACs materials, and facilitate their practical applications.

2. Catalytic mechanism of SACs in cathodes for Li-S batteries

The electrochemical reaction process of Li-S batteries during discharge can be summarized by the equation $16Li + S_8 \rightarrow 8Li_2S$ [42]. But in the specific discharge process, the reaction is very complicated. (i) Conversion from solid S_8 to liquid Li_2S_8 ($S_8 \rightarrow Li_2S_8$), (ii) from liquid Li_2S_8 to Li_2S_4 ($Li_2S_8 \rightarrow Li_2S_6 \rightarrow Li_2S_4$), and (iii) from liquid Li_2S_4 to solid Li_2S_2 and Li_2S ($Li_2S_4 \rightarrow Li_2S_2 \rightarrow Li_2S$), shown in Fig. 2a [43]. These two solid-liquid phase conversion reactions also correspond to the two discharge platforms in Fig. 2b. More specifically, one of the most serious problems in Li-S batteries is the shuttle effect of LiPSs during the reaction process, which reduces the utilization of sulfur. Moreover, the electronic and ionic conductivity of the discharge products Li_2S_2 and Li_2S is not good, which reduces the overall conversion reaction kinetics of the Li-S battery. Hence, exploring reasonable strategies to solve the shuttle problem of LiPSs and rapid conversion between polysulfide is of great significance for improving the performance of Li-S batteries [44]. SACs have played an important role in solving these problems.

Catalysts can significantly improve the electrochemical reaction process of batteries [45,46]. However, because of the complexity of nanoscale catalysts, it is hard to get close to the reality of the situation. SACs have definite active sites and have been widely stud-

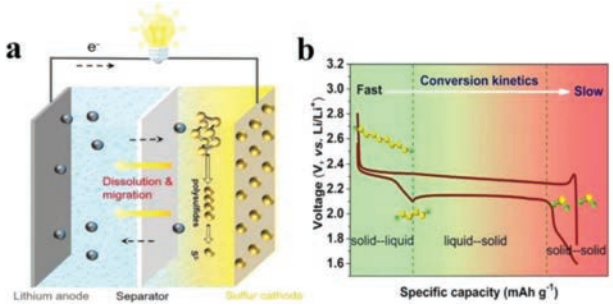

Fig. 2. (a) Schematic diagram of Li-S batteries charging and discharging reaction mechanism. (b) Li-S batteries charging and discharging voltage curve. Adapted with permission [35]. Copyright 2020, Wiley-VCH.

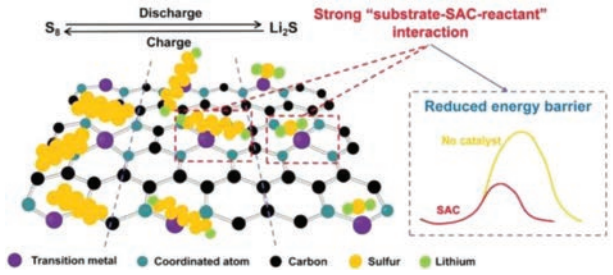

Fig. 3. Catalytic mechanism of SACs in the cathode of Li-S batteries. Adapted with permission [41]. Copyright 2021, Elsevier.

ied in recent years [47]. SACs are usually dispersed into carbon materials and anchored by adjacent coordinating atoms [48]. The catalytic mechanism of SACs in Li-S battery cathodes is shown in Fig. 3. There is a Lewis acid-base interaction both LiPSs and SACs [49]. During the discharge process, SACs will preferentially chemically adsorb with LiPSs and form an intense interaction with LiPSs, which can greatly reduce the energy required for the reduction process. In addition, Li_2S_8 is rapidly reduced to Li_2S, which suppresses the diffusion of LiPSs [41,50]. Finally, Li_2S products are uniformly deposited on the substrate. During the charging process, SACs can reduce the energy needed for Li_2S decomposition, thus reducing the polarization voltage in the battery reaction process, improving the overall kinetics of the chemical reaction, and improving sulfur utilization.

Researchers have also verified this by theoretical calculations [51–54]. Recently, Zhou and co-workers used theoretical simulation to screen SACs materials for catalytic decomposition of Li_2S. Considering the diversity of metal atoms, eight SAs (Fe, Mn, Ru, Zn, Co, Cu, V and Ag) on NG material were chosen. The decomposition pathways of Li_2S on different substrates were calculated, as shown in Fig. 4a. The results indicated that the decomposition barrier of materials with SACs was lower than that of graphene. Among all the materials screened, they discovered that SAV@NG had the smallest decomposition barrier for Li_2S_6, and the structural stability and anchoring effect is the best. Thus, V SACs were selected as the investigated SACs. Moreover, they synthesized graphene materials with V SACs. The cathode materials achieved a high discharge capacity of 645 mAh/g at a rate of 3 C and stabilized at ~485 mAh/g after 200 cycles. In addition, this material has excellent rate performance and reversibility. The electrode can recover to its original capacity when the current rate suddenly returns to the rate of 0.5 C, as shown in Fig. 4b. The electron transformation behavior between Li_2S and the substrate has also been considered. In addition to the electron transfer between the Li atom and the substrate materials, there is also a large amount of electron transfer between the S atoms and SAs. The bonds between S atoms and the metal atoms further weaken the Li-S bond, thus reducing the decomposition barrier of Li_2S. This reduces the decomposition barrier of LiPSs/Li_2S, as shown in Fig. 4c [55]. Their work reveals the mechanism of SACs and has implications for the selection of different SACs in Li-S batteries.

3. Strategies of synthesizing SACs in cathodes for Li-S batteries

There are many ways to synthesize SACs, but almost all researchers have used high-temperature pyrolysis methods to synthesize cathode SACs for Li-S batteries [41]. In high-temperature pyrolysis, precursors usually contain the target substances including compounds containing SAs. They are mixed and then pyrolyzed in the usual temperature range from 600 °C to 1100 °C [30]. In addition, different precursors are usually used when pyrolyzing metal-organic complexes, which have the characteristics of molecular confinement and coordination of organic ligands [43]. Moreover, the pyrolysis process enormously enhances the stability of metal SAs. This helps to increase the SAs loading and improve the catalytic durability [56,57]. However, when metals are separated into isolated SAs, their surface free energy is greatly increased, making the SAs prone to aggregation during preparation and electrochemistry [58,59]. In order to prevent this phenomenon, two strategies are commonly used to disperse and stabilize SAs during the preparation process, namely the spatial confinement strategy and the coordination design strategy. In this section, we describe both strategies in detail.

3.1. Spatial confinement strategy

The spatial confinement strategy involves keeping SAs are kept in a molecular-scale cage to avoid migration [60]. Metal-organic frameworks (MOFs) are suitable substrates for stabilizing SACs [41,61]. MOFs are widely regarded as good sacrificial templates for the manufacture of porous materials since they include all of the critical ingredients required for the preparation of SAs [62]. And the porous structure gives the material a large surface area. The metal compound can be turned into SAs after high-temperature treatment, and the SAs can be successfully anchored and restricted in the porous host materials [30]. For example, Wang *et al.* suggested SAs Fe catalysts anchored on nitrogen-rich MOF-derived carbon cages (FeSA-CN) as a steady and high efficient cathode host for Li-S batteries. They chose zeolite imidazoline framework-8 (ZIF-8) as the precursor, due to its excellent channel structure and inherent nitrogen elements, which can anchor Fe atoms well. The sample was moved to a tube furnace and pyrolyzed in argon atmosphere. Finally, cooled the sample to room temperature to obtain FeSA-CN, as shown in Fig. 5a [34]. Moreover, the FeSA-CN materials have a uniform dodecahedron structure consistent with the initial structure (Fig. 5b). The highly porous structure of the isolated SAs Fe catalyst was revealed by high-resolution transmission electron microscopy (HRTEM), as shown in Fig. 5c. And the isolated SAs Fe catalyst was randomly dispersed on the nitrogen-rich carbon cage by high-angle annular dark-field scanning transmission electron microscopy (HAADF-STEM), as shown in Fig. 5d. Later on, Li and co-workers fabricated SAs Co catalysts (CoSA) on conductive NC nanosheet (CoSA-N-C) materials *via* the salt template strategy. The cobalt(II) precursor and 2-methyl imidazole (2-MIM) form coordination at 70 °C, and grow a cobalt zeolite imidazole framework (ZIF-67) on the surface of potassium chloride (KCl) particles to obtain ZIF-67@KCl. The ZIF-67@KCl precursor was then annealed at 750 °C for 2 h in an argon atmosphere, then washed in a hydrochloric acid solution to obtain the final SACs materials (CoSA-N-C) [63]. SACs can employ the extensive coordination sites created by pyrolysis as anchor sites.

In addition to MOF structures, self-assembled micro-cages are often used to disperse SAs. For instance, Shao *et al.* synthesized

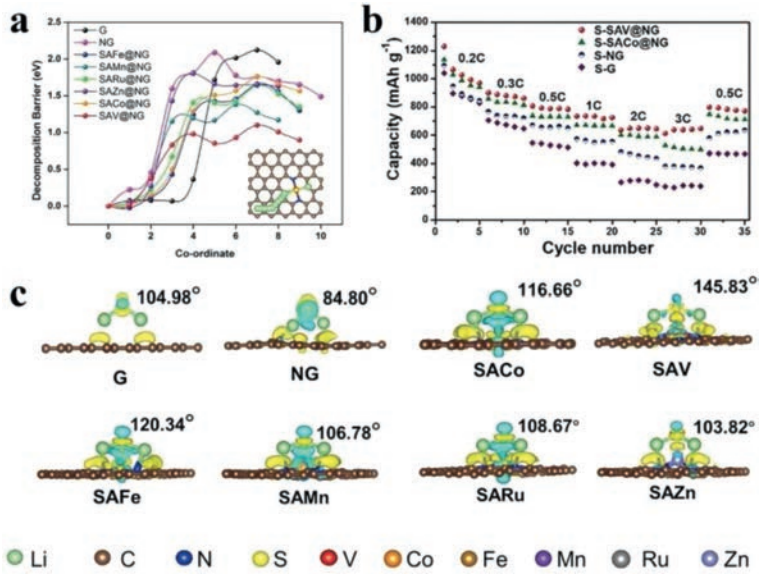

Fig. 4. (a) Decomposition barriers of Li_2S and (c) the differences in charge density of Li_2S adsorption on different substrates: grapheme (G), NG and single atoms (SAs) Fe, Mn, Ru, Zn, Co and V on N-doped graphene (NG) materials. (b) The S-G, S-NG, S-SACo@NG and S-SAV@NG electrodes rate performance. Adapted with permission [56]. Copyright 2020, American Chemical Society.

mesoporous hollow carbon spheres (MHCS), and then heated them under a gas flow of Ar and NH_3 to obtain N-doped MHCS. Subsequently, iron phthalocyanine solution containing tetrahydrofuran was added to get the precursor, followed by centrifugation and drying. Finally, the sample was pyrolyzed to get Fe-N/MHCS materials (Fig. 5e) [31]. The Fe-N/MHCS material maintained the spherical shape and the integrity of the mesoporous carbon shell, as shown in Figs. 5f and g. The absence of Fe nanoparticles was also revealed by transmission electron microscopy (TEM) pictures of the Fe-N/MHCS (Fig. 5h). This further proves that iron exists in the form of SAs.

3.2. Coordination design strategy

The coordination design strategy uses the stable bonds formed between SAs and coordination atoms to tightly bind individual metal atoms together, which is the key to preventing agglomeration [60]. A variety of carbonaceous materials have been suggested to load sulfur because of their ability to increase the electrical conductivity of cathode materials and physically prevent polysulfides [64]. Nevertheless, SAs tend to aggregate when dispersed into carbon host materials, and polar LiPSs are anchored to nonpolar carbon materials through van der Waals forces, and the force between them is very weak. Moreover, the polar–polar interaction is a strong chemical interaction between polar LiPSs and polar host materials that can be tuned to adsorb LiPSs [65]. Because of their lone pairs, nitrogen (N), oxygen (O) and sulfur (S) are excellent choices for doping in a carbon matrix, and they can trap SAs. Recently, N-doped C-based materials have also been researched for dispersing SACs. For example, Du *et al.* synthesized cobalt SACs embedded in nitrogen doped carbon (Co-N/G) materials. They added 1 mL of aqueous solution of $CoCl_2$ $6H_2O$ into a graphene oxide (GO) suspension to acquire a precursor. Finally, the precursor was pyrolyzed to obtain Co-N/G [39].

The upper threshold of N doping concentrations (~14.5 at%) limits the improvement of these materials [66]. Graphitic carbon nitride (g-C_3N_4) and C_3N_4 have extremely high nitrogen contents and are also used as host materials of dispersed SACs. For example, Lu *et al.* used simple methods to disperse iron SAs into g-C_3N_4 (SAFe@g-C_3N_4). Firstly, the g-C_3N_4 material and iron(II) acetate were dispersed into the ethanol solution to obtain the precursor. Subsequently, the precursor was pyrolyzed to obtain SAFe@g-C_3N_4, as shown in Fig. 6a. The SEM image in Fig. 6b shows the layered structure of the SAFe@g-C_3N_4 material. A large number of single iron atoms were uniformly dispersed in the SAFe@g-C_3N_4 material (Figs. 6c and d). This coordination effect leads to high SAs loading, achieving as high as 8.5 wt% in the SAFe@g-C_3N_4 materials [67]. Following this concept, Wu and co-workers used the same method to prepare Co@C_3N_4 [68].

However, ultra-high concentrations of nitrogen also reduce electrical conductivity. Zhao *et al.* proposed N and S dual-doped nanoporous carbon as a precursor of SACs. Firstly, the solution was freeze-dried in liquid nitrogen. The obtained material was calcined in an Ar atmosphere, washed, and dried to obtain FeNSC. They demonstrated that the synergistic effect of SAs Fe and doped sulfur accelerates the reversible conversion of electrochemical reactions in Li-S batteries [21].

3.3. Summary

Based on the above mentioned studies, the spatial confinement and coordination design strategies allow single metal atoms to be evenly dispersed over the host materials. Among them, the SACs obtained by the space confinement strategy has the advantages of uniform distribution and clear structure. However, this method usually requires high-temperature pyrolysis and strict reaction conditions to remove ligands in the precursor and generate micro cage for trapping SAs, which limits large-scale production [60]. Compared with the spatially constrained strategy, the coordinated design strategy can control the coordination structure, the number of anchored metal atoms, and the interactions between metal atoms and ligands. It helps to synthesize various SACs with well-controlled structures and functions [53]. With a combination of the two strategies to disperse the SACs, the dispersion effect is better and further improves the loading of the SACs. Moreover, when the SACs are more evenly dispersed and loaded, they can improve the chemical kinetics and utilization of the active S of the Li-S batteries.

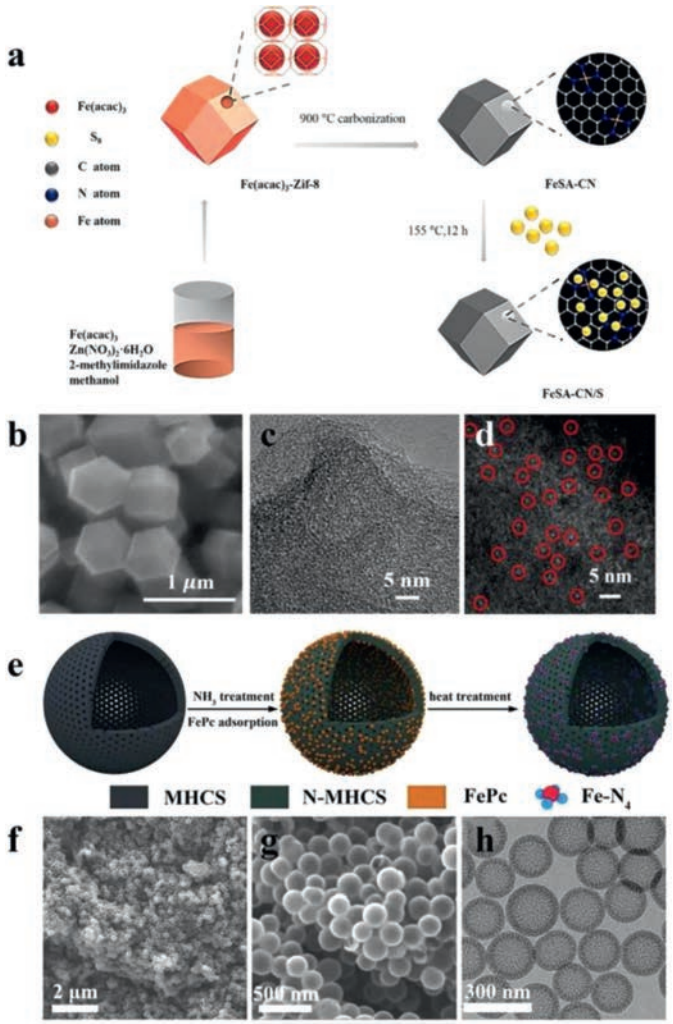

Fig. 5. (a) Process of synthesizing FeSA-CN/S material. SAs Fe anchored on nitrogen-rich MOF derived carbonaceous cage (FeSA-CN) imaged using (b) Scanning electron microscopy (SEM) and (c) high-resolution transmission electron microscopy (HRTEM). (d) FeSA-CN/S imaged using high-angle annular dark-field scanning transmission electron microscopy (HAADF-STEM). (e) Process of synthesizing SAs Fe embedded N-doped mesoporous hollow carbon spheres (Fe-N/MHCS) nanoreactors. (f, g) SEM and (h) transmission electron microscopy images (TEM) of Fe-N/MHCS. (a–d) Adapted with permission [34]. Copyright 2020, Royal Society of Chemistry. (e–h) Adapted with permission [31]. Copyright 2020, Royal Society of Chemistry.

4. Application of SACs in the cathodes of Li-S batteries

The sulfur cathode is one of the most critical components in a Li-S battery because it impacts the complete cell's energy density, rate performance, and cycle stability [40]. SACs have unique coordination characteristics and active centers, which have great advantages in battery applications. They can accelerate the chemical reaction process of batteries and improve the utilization of sulfur [69,70]. In this section, we review the applications of different SACs in the cathodes of Li-S batteries, including iron, cobalt, and zinc. More information about the applications of SACs in the cathodes of Li-S batteries is shown in Table 1.

4.1. Single-atom Fe catalysts

In recent years, SAs Fe has been reported as a catalyst in oxygen reduction, carbon dioxide reduction, and hydrogen evolution. Inspired by this, the first SACs used in the cathode of Li-S battery were Fe atoms [43]. Through polymerization and pyrolysis of diphenylamine with iron phthalocyanine and a hard template, Liu *et al.* created a porous NC host with abundant SAs Fe sites (Fe-PNC). They demonstrated that the cathode with SAs Fe catalysts can improve the conversion of LiPSs in Li-S batteries during charging and discharging (Fig. 7a). The single Fe atoms were more or less evenly distributed, as shown in Fig. 7b. And Mössbauer spectroscopy further demonstrated that the Fe atoms were scattered in the NC layers (Fig. 7c). Compared with pure PNC, Fe-PNC/S composite materials have higher capacity and better cycle stability. Batteries fabricated with Fe-PNC/S composite materials showed an initial specific capacity of 1138.6 mAh/g at a rate of 0.1 C and a discharge capacity of 427.1 mAh/g after 300 cycles, with capacity decay per cycle was ~0.2%. Moreover, Fe-PNC/S composite materials had a greater capacity (557.4 mAh/g) after 300 cycles at 0.5 C (Fig. 7d). This is due to the accelerated conversion of LiPSs in Li-S batteries under the catalysis of SAs Fe. Meanwhile, the rapid electrode reaction helps to reduce the dissolution of LiPSs in the electrolyte. Hence, through the catalysis of SAs Fe, the conversion of LiPSs is accelerated, and the performance of FePNC/S batteries is significantly improved. By enhancing polysulfide conversion, the catalytic effect significantly improved the electrochemical performance of Fe-PNC/S cells [38]. This groundbreaking work opened a new path toward efficient LiPSs conversion, and more people are researching the use of SACs in Li-S batteries.

Following this concept, Shao and co-workers proposed a method for dispersing single Fe atoms in nitrogen-containing

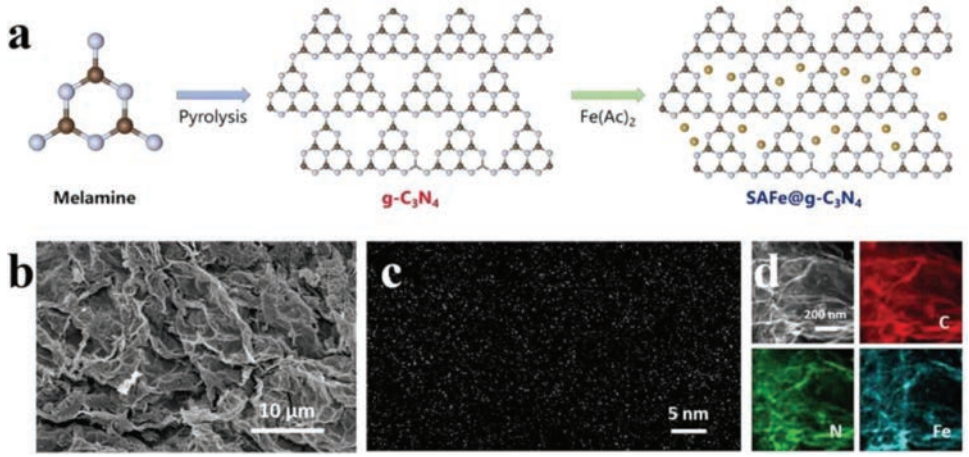

Fig. 6. (a) Process of synthesizing SAs Fe dispersed on g-C_3N_4 (SAFe@g-C_3N_4) materials. (b) SEM images and (c) HAADF-STEM of SAFe@g-C_3N_4 material. (d) Energy dispersive X-ray (EDX) mapping of SAFe@g-C_3N_4 material. Adapted with permission [71]. Copyright 2020, American Chemical Society.

Table 1
Summary of the application of SACs in the cathodes of Li-S batteries.

Sample	Configuration	Content of SAs	Initial capacity (mAh/g) at (x) rate	Capacity (mAh/g) after (n) cycles at (x) rate	Maximum S loading (mg/cm^2)	Sulfur content (wt%)	E/S ratio (μL/mg)	Ref.
FeNSC	Fe–N and Fe–S	3.2 wt%	1306 (0.05)	477.1 (1000) (1.0)	1.0	65		[21]
Fe-N/MHCS	Fe–N	1.03 wt%	1185 (0.1)	834 (1000) (1.0)	5.4	80	8.0	[31]
FeSA-CN	Fe–N	1.14 wt%	1123 (0.2)	796 (200) (0.5)	6.0	68.7	20	[34]
Fe-PNC	Fe(II)–N_4	1.0 wt%	1138.6 (0.1)	427 (300) (0.1)	1.3	70		[38]
Co-N/G	Co-N_4	0.77 at%	1210 (0.2)	681 (500) (1.0)	6.0	90	20	[39]
SAV@NG	V-N	4.3 wt%	1230 (0.2)	551 (400) (0.5)	5.0	80		[55]
CoSA-N-C	Co-N_4	15.3 wt%	1574 (0.05)	675 (1000) (1.0)	4.9	74.2	10.4	[63]
SAFe@g-C_3N_4	Fe–N	8.5 wt%	1379 (0.1)	1129 (200) (0.2)	2.3		3.8	[67]
Co@C_3N_4	Co–N		1400 (0.5)	980 (200) (1.0)	4.0		21	[68]
Fe-N_5–C	Fe-N_5	0.0188 wt%	1224 (0.2)	662 (500) (1.0)	8.2	74	8.9	[69]
HFeNG	Fe–N_4 and Fe–N_2		1298 (0.2)	1100 (300) (0.5)	5.0	86.5	10 mL/g	[70]
Co-CMP	Co−N/O	2.32 wt%	1440 (0.1)	549 (1000) (0.5)	4.7	83.8	20	[72]
Co–N_4@2D/3D Carbon	Co–N_4	1.01%	1171 (0.2)	1000 (100) (0.2)	4.6	73	15	[73]
Co-SAs@NC	Co-N_4	0.66 wt%	1438 (0.1)	1059 (100) (0.2)	5.0	76		[78]
SA-Zn-MXene		1.5 wt%	1136 (0.2)	706 (400) (1.0)	5.3			[80]
Zn_1–HNC	Zn-N_4	15.7 wt%	1225 (0.5)	1214 (100) (0.5)	7.8		6.4	[81]
SATi@CF	Ti–N and Ti–O	1 wt%	1151 (0.2)	845 (300) (0.5)	8	65	10	[82]
Mn/C-(N, O)	Mn-N and Mn-O	0.36%	1330 (0.2)	560 (600) (0.5)	4.0	76		[85]
Ni−N_5/HNPC	Ni−N_5	0.6 wt%	1086 (0.5)	798 (500) (0.5)	5.1			[86]
Co-NG(800)	Co–N_4	2.50 wt%	972 (0.5)	505 (600) (0.5)	11.8	74		[88]

1 C = 1675 mAh/g based on S weight; E/S ratio = electrolyte/sulfur ratio.

mesoporous carbon hollow spheres (Fe-N/MHCS). Through experimental and theoretical calculations, it has been confirmed that the Fe-N_4 center has good catalytic activity, which can promote the reversible conversion of both LiPSs and Li_2S and regulate the deposition of Li_2S. Moreover, even under high S load and low E/S ratio, the area capacity achieved 6.4 mAh/cm^2 and retained 81.7% after 100 cycles. In addition, the S@Fe-N/MHCS pouch cell was also made, and the capacity retention rate of the battery after 200 cycles was as high as 77.1% [31]. Recently, Zhao *et al.* prepared FeNSC by high-temperature pyrolysis, as shown in Fig. 7e [21]. The transmission electron microscopy image of FeNSC shows the morphology of the porous nanosheets (Fig. 7f). And the HAADF-STEM images also show that the single Fe atoms are uniformly scattered in the host material (Fig. 7g). The FeNSC/S cathodes showed an initial specific capacity of 1306 mAh/g at a rate of 0.05 C and it had good reversibility, as shown in Fig. 7h. This work makes effective use of the synergy between metal and non-metal materials. It proposes a novel strategy to the development of high-performance Li-S batteries. In addition to loading SACs on NC, Wang and co-workers used nanocage-like nitrogen-rich MOFs to derive a FeSA-CN catalyst to trigger LiPSs' surface-mediated reactions. ZIF-8 was selected as a precursor to anchor the catalyst Fe because of its outstanding pore structure and inherently high nitrogen concentration. The results showed that LiPSs might be adsorbed into FeSA-CN materials. FeSA that is dispersed at random could speed up the conversion of LiPSs. And at 0.2 C, the FeSA-CN/S electrodes could yield 1123 mAh/g of capacity. Theoretical and experimental results showed that nitrogen-rich MOF structures loaded with FeSA catalysts could accelerate the reversible transformation reaction during charging and discharging and ensured cycling stability during long-term cycling [34].

4.2. Single-atom Co catalysts

In addition to the SAs Fe used as catalysts for the cathode material of Li-S batteries, SAs Co has also been studied as catalysts in Li-S batteries [71–73]. The strong Co–S bond formed by the interaction between Co and S promotes the transformation of polysulfides [68,74,75]. Du and co-workers discovered that Co-N/G could greatly accelerate the conversion of LiPSs. Combined with operand X-ray absorption spectroscopy and first-principle calculations, they revealed that the Co-N-C coordination center functions as a bifunctional electrocatalyst to promote the creation and breakdown of Li_2S during discharge and charge, respectively. Therefore, at a high S mass loading of 6.0 mg/cm^2 in S@Co-N/G electrodes, the composite delivered an area capacity of 5.1 mAh/cm^2 at 0.2 C. During 100 cycles, the performance remained steady, with a capacity decay rate of 0.029% per cycle. Moreover, Li_2S is produced only toward the end of the second discharge plateau on carbon, according to prior X-ray absorption neat-edge structure (XANES) studies.

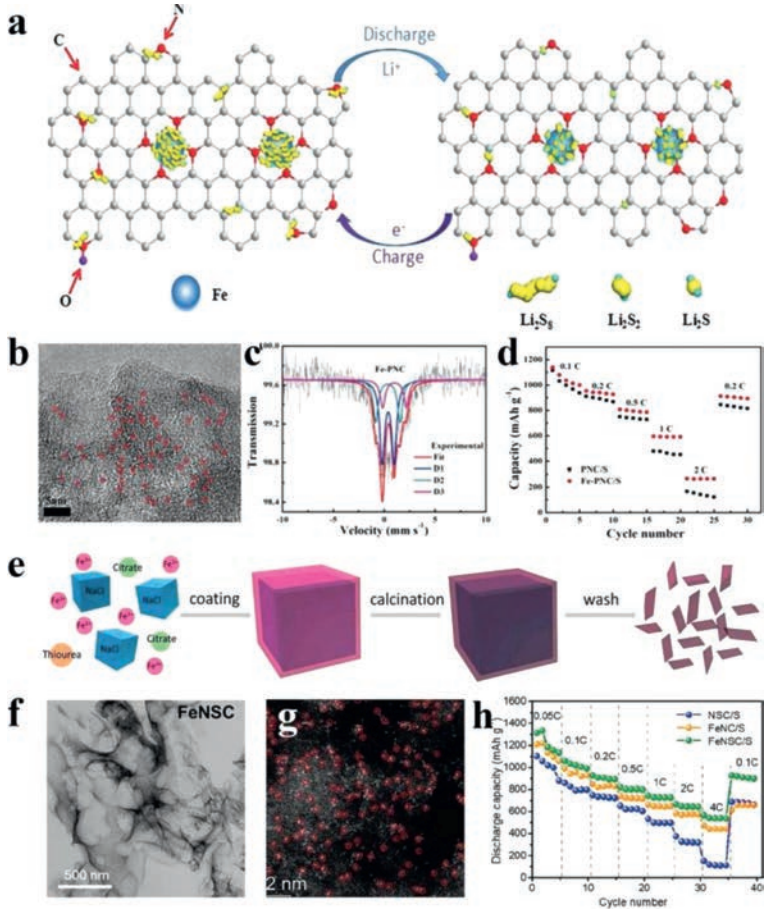

Fig. 7. (a) The conversion of LiPSs on the Fe-PNC surface is depicted schematically. (b) HRTEM images of Fe-PNC. (c) Fe-PNC transmission spectra for ^{57}Fe Mössbauer at 293 K. (d) PNC/S and Fe-PNC/S material rate performances at various current densities. (e) Process of synthesizing FeNSC material. (f) TEM images of FeNSC. (g) HAADF-STEM images of FeNSC. (h) Rate capabilities of NSC/S, FeNC/S, and FeNSC/S. (a–d) Adapted with permission [38]. Copyright 2018, American Chemical Society. (e–h) Adapted with permission [21]. Copyright 2021, American Chemical Society.

Remarkably, Du and co-workers observed the creation of Li_2S at the first stage of discharge through an operand XANES experiment [39].

Later on, Wu *et al.* implanted Co SACs onto another frequently used host material, namely carbon nitride (C_3N_4). This was created by reacting melamine with cyanuric acid in the presence of Co^{2+}, as shown in Fig. 8a [68]. Furthermore, the absorption edge of Co K-edge XANES was close to but slightly higher than that of CoO, indicating that Co is between bivalent and trivalent at Co@C_3N_4 (Fig. 8b). Co is dispersed on the host material as a single atom, according to the Fourier transform extended X-ray absorption fine structure of Co@C_3N_4 (Fig. 8c). The cathode with Co SACs had a large specific capacity of ~1400 mAh/g at 1.6 mA/cm^2. The cycling stability with 4 mg/cm^2 of sulfur was 2 mA/cm^2 after 200 cycles and its capacity remained at ~780 mAh/g (Fig. 8d). It has been reported that the proportion of SACs in the matrix material is very low (usually <5 wt%) [20]. In order to improve battery performance, researchers hope that the matrix material can provide a lot of active sites to support SACs [76]. Li *et al.* used a salt template method to produce single Co atoms inserted in NC nanosheets, and the Co content was up to 15.3 wt%. The dense Co-N_4 coordination center acted as a catalytic site to speed up the reversible conversion between LiPSs and Li_2S. More vital, the CoSA-N-C material realizes the uniform deposition of Li_2S nanoparticles and catalyzes the oxidation of Li_2S. As a result, the CoSA-N-C@S electrode could deliver a high specific capacity of 624 mAh/g at 5 C and a fading rate of 0.035% per cycle over 1000 cycles at 1 C [63].

MOF materials are also used to disperse SACs [77]. For example, Li *et al.* used binary Co-Zn MOF precursors to successfully disperse SAs Co into NC materials (Co-SAs@NC) (Fig. 8e) [78]. In binary Co-Zn ZIF-precursor (Co_1Zn_1-BZIF), because of the identical coordination of Co^{2+} and Zn^{2+} with 2-methylimidazole, Co and Zn are uniformly distributed [79]. The morphology of Co_1Zn_1-BZIF did not change after pyrolysis, as shown in Fig. 8f. The oxidation state of SAs Co is closer to Co^{2+}, according to the XANES spectrum of Co. This shows that SAs Co sites have a porphyrinic planar structure, as shown in Fig. 8g. The cyclic voltammetry of a symmetric cell with four symmetrical reversible anodic and cathode peaks was tested to acquire experimental evidence of the electrocatalytic activity of Co-SAs@NC for LiPSs transformation (Fig. 8h). Nitrogen coordination is essential for preventing the coalescence of single Co atoms and providing catalytic activity for the conversion of LiPSs to Li_2S. The S@Co-SAs@NC cathode could operate 600 cycles at 1 C with a sulfur load of 2.0 mg/cm^2, providing a steady capacity of 737 mAh/g. Furthermore, this research indicates potential uses in catalysis and other electrochemical cells.

4.3. Single-atom Zn catalysts

In recent years, the use of Fe and Co SACs in Li-S batteries has been widely studied, but Zn has been relatively less researched. However, the working principle is actually similar. Recently, Zhang's group fabricated SA-Zn-MXene layers by etching Al layers of MAX (Ti_3AlC_2) in molten zinc chloride (600 °C) [80]. Because of the strong electronegativity of atomic zinc on Mxene, this

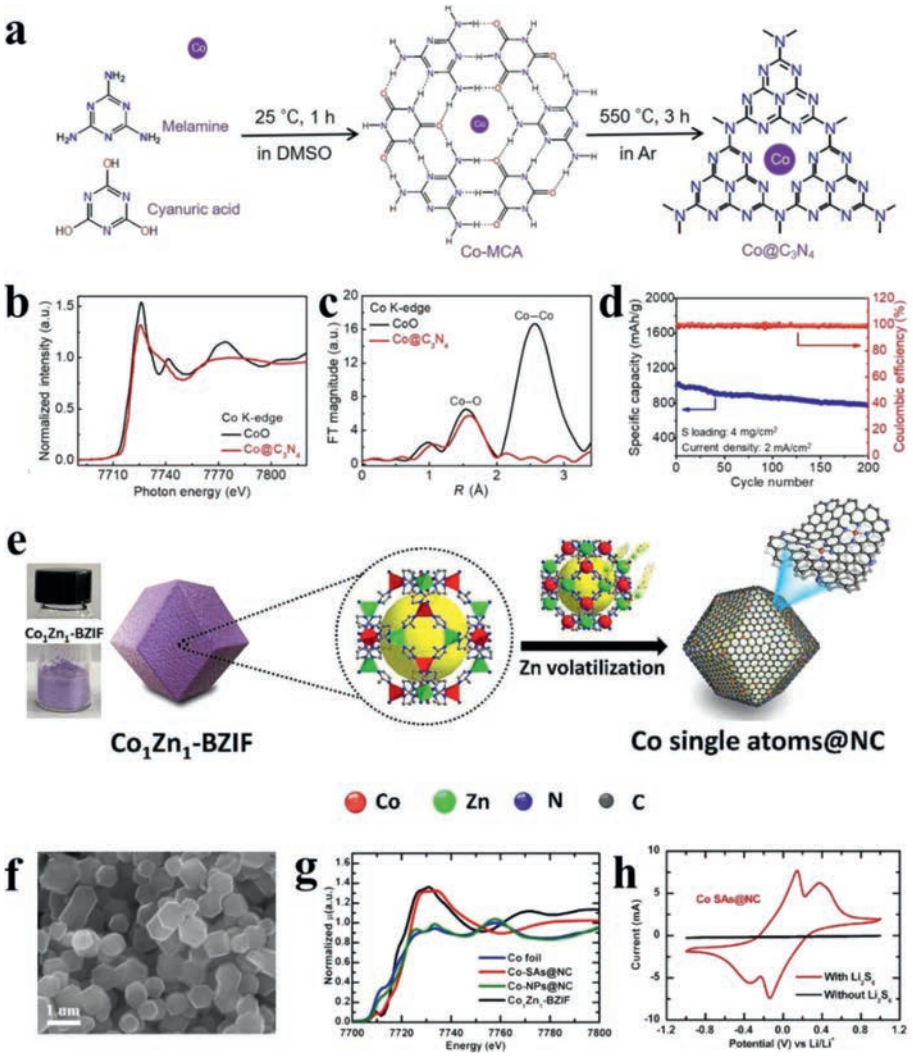

Fig. 8. (a) Process of synthesizing Co@C_3N_4 material. (b) Co K-edge XANES and (c) the matching extended X-ray absorption fine structure of Co@C_3N_4. (d) Li-S battery cycling stability employing Co@C_3N_4 as the cathode electrocatalyst. (e) Process of synthesizing SAs Co supported on NG material. (f) SEM image of the Co_1Zn_1-BZIF. (g) Co K-edge XANES spectra. (h) Cyclic voltammetry profiles of symmetrical cells for electrodes of Co-SAs@NC. (a–d) Adapted with permission [68]. Copyright 2019, Elsevier B.V. and Science China Press. (e, f) Adapted with permission [78]. Copyright 2020, Elsevier.

not only promoted the conversion of polysulfides by reducing the energy barrier between Li_2S_4 and Li_2S_2/Li_2S, but also had a strong affinity for polysulfides. As a result, at 6 C, the sulfur cathode with SAs zinc implanted MXene demonstrated a high reversible capacity of 1136 mAh/g and a decent rate capability of 640 mAh/g. It also showed good cycle stability after 200 cycles at 4 C it can have 80% capacity retention.

Later, Shi's group synthesized a dual-functional single atom Zn-decorated hollow carbon spheres (Zn_1–HNC) nanoreactor by pyrolysis of the hollow-structured ZIF-8 precursor under Ar protection (Fig. 9a) [81]. Moreover, the single Zn atoms can load up to 15.7% because of the massive homogeneously dispersed single atom clusters and the abundant porous structure, as shown in Fig. 9b. The redox kinetics of the LiPSs was outstandingly enhanced, and dendrite growth was significantly suppressed. The fully fabricated Li-S batteries (Zn_1–HNC-S||Zn_1–HNC-Li) showed a good rate performance of ~989 mAh/g at 10 C and a low capacity fading rate of 0.015% per cycle over 700 cycles at 5 C. Even with an S mass loading of 7.8 mg/cm^2, a low E/S ratio of 6.4 μL/mg, and an N/P ratio of 1.8:1, this full battery still delivered a high area capacity of 8.7 mAh/cm^2. In addition, this battery maintained a stable discharge capacity of 1149 mAh/g after 300 cycles (Fig. 9c). This work provided significant insight into the structure and surface catalytic chemistry regulation for promoting the actual application of Li-S batteries.

4.4. Others

Alongside these three metals, many other SACs can be used as catalysts [82]. For example, Zhang and co-workers proposed design principles for using chemically functional graphene as an anchoring material to achieve enhanced chemical trapping and catalysis. Its periodic law can theoretically be calculated from first principles. Seven different co-doped series such as MN_4@graphene (M = V, Cr, Mn, Fe, Co, Ni, and Cu) have been investigated. As a consequence, FeN_4 and CrN_4 co-doped graphene has strong anchoring and catalytic effects for Li-S batteries [83]. Metal-N_4/graphene plays a key role in immobilizing soluble Li_2S_n to host materials to restrain the shuttling effects and improve the rate and cycling properties [52]. Later on, Song and co-workers constructed metal phthalocyanine and covalent organic framework (COF) materials (MPc-COFs, M = Ti, V, Mn, Cu, Zn) as cathodes. The advantages of metal atoms and COFs were integrated in this material. The adsorption and catalytic properties of the MPc-COFs cathode for Li_2S_x species were inves-

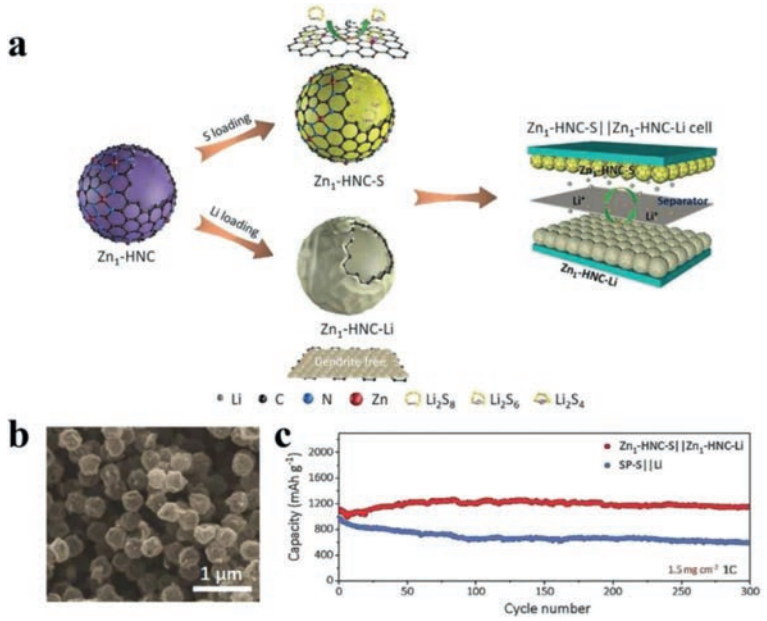

Fig. 9. (a) Process of synthesizing the dual-functional Zn_1–HNC nanoreactors of the full Zn_1–HNC-S||Zn_1HNC-Li battery. (b) SEM image of Zn_1–HNC. (c) Cycling stability of Zn_1–HNC-S||Zn_1–HNC-Li batteries. Adapted with permission [81]. Copyright 2020, Wiley-VCH.

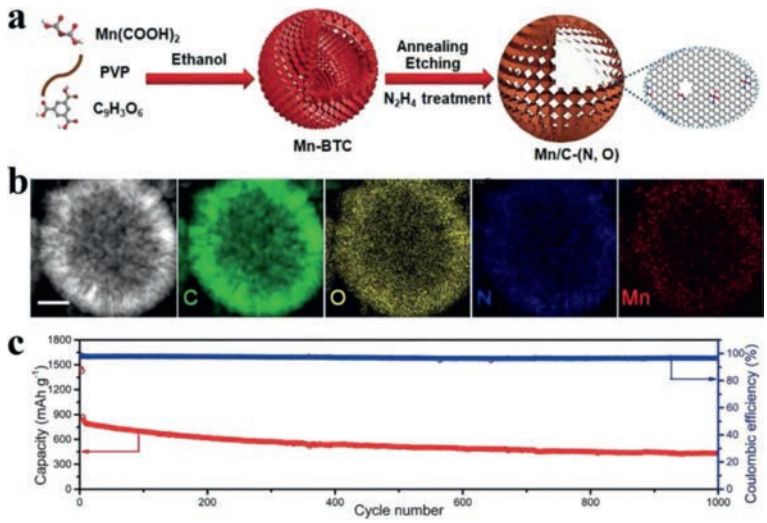

Fig. 10. (a) Process of synthesizing the Mn/C-(N, O). (b) Mn/C-(N, O) HAADF-STEM pictures and elemental mapping images of C, O, N and Mn. (c) S@ Mn/C-(N, O) cycling performance. Adapted with permission [85]. Copyright 2020, Elsevier.

tigated by density functional theory. The Bader charge and partial density of states analyses revealed that there are Li-N and S-M interactions between Li_2S_x species and MPc-COFs, with the S-M interaction accounting for the majority of the system adsorption energy. And the adsorption capacity of TiPc-COF and VPc-COF is too strong, forming an axial complex, which is unfavorable for Li-S batteries. Finally, MnPc-COF shows excellent conductivity and sulfur fixation capacity, and also has a lower energy barrier in the catalytic oxidation of Li_2S [84].

Recently, Liu and co-workers successfully introduced single manganese (Mn) atoms into a hollow carbon sphere framework co-doped with O and N atoms (Mn/C-(N, O)) by pyrolysis (Fig. 10a) [85]. MOF-derived carbon can be used as a support to induce the embedding of SAs Mn in the carbon framework, which allows SAs Mn to be distributed more evenly. The elements are evenly distributed throughout the material, as shown in Fig. 10b. Moreover, the coordination of SAs Mn with O and N can further stabilize the Mn atoms, so that the material has abundant atomic active sites. And SACs Mn can enhance the Lewis acid-base interaction to better anchor LiPSs. In addition, SAs Mn can accelerate the conversion of LiPSs. Finally, Mn atoms serve as polar adsorption sites and catalytic activity centers, which can shorten the reaction path and further increase the reaction rate. Therefore, the battery using S@Mn/C-(N, O) composite material shows good rate performance of 900 mAh/g at 1 C and a low capacity fading rate of 0.05% per cycle over 1000 cycles at 1 C (Fig. 10c).

Very recently, under the guidance of theoretical calculations, Zhang *et al.* constructed a multifunctional catalyst of SAs Ni dispersed in hollow nitrogen-doped porous carbon (Ni−N/HNPC) as an ideal carrier for the sulfur cathode. They emphasized the important role of the coordination number of the active center in the SACs, and through the energy distribution test of the discharge process from S_8 to Li_2S, they found that the materials with Ni-N_5 as the active center have the best catalytic effect. Therefore, the battery using Ni−N_5/HNPC/S composite material shows a good rate

performance of 1086 mAh/g at 0.5 C and a low capacity fading rate of 0.053% per cycle over 500 cycles at 0.5 C [86].

4.5. Summary

Based on the review above, we can clearly see that the SACs used for the sulfur cathodes of Li-S batteries can catalyze the conversion of insoluble Li_2S to enhance the utilization of S, as well as the conversion of LiPSs to lessen the shuttle effect. First, the SACs have a large atom utilization ratio and a definite active site, which can better capture and catalyze the LiPSs and improve the chemical kinetics of Li-S batteries. Moreover, the local coordination of SACs can be clearly characterized by advanced microscopy, which helps understand the reaction mechanism at the atomic scale. Finally, SACs can reduce the energy required for the conversion of Li_2S_2/Li_2S to S and can increase the utilization of active S. Moreover, the stability of SACs sites during long-term cycling in Li-S batteries have been investigated by a few groups [87,88]. For example, Meng *et al.* reported that aggregates of SACs Co attached to graphene *via* porphyrins. Atomic-resolution transmission electron microscopy and X-ray absorption spectroscopy measurements show that the Co atoms present in the SACs aggregates exist as SAs. And through the Co K-edge XANES spectrum test of the S@Co-NG cathode in different electrochemical states, it is found that over the charge/discharge cycle, the absorption edge remained consistently at a higher region along with largely unchanged spectroscopic features. These results indicated that the structure of the single-atom Co aggregates was essentially unchanged during the charge/discharge cycle and that interactions formed between the Co SACs and the sulfur species persisted throughout the electrochemical process [88]. In the future, futher research is needed on the inactivation mechamism and regeneration of SACs in Li-S batteries.

In addition, the catalytic activities of different types of SACs in Li-S batteries also have significant differences [89]. Recently, Cai and co-workers studied the catalytic performance of four SACs materials formed with $TM-N_4-C$ (TM = Co, Fe, V and W) through simulations based on density functional theory. The SACs reduce the Li_2S_2 to Li_2S reaction energy by over 1.0 eV, compared to pristine graphene. Among the four SACs materials, Co-N_4–C and Fe-N_4–C show similar LiPSs adsorption energy and activation energy for Li_2S_2 to Li_2S conversion, while V-N_4–C and W-N_4–C show greater adsorption energy and catalytic activity. And comparable to $V-N_4-C$, $W-N_4-C$ is shown to be a promising electrocatalyst and cathode material for Li−S batteries as it gives the highest LiPS adsorption energies and high catalytic activity [54]. And Zhou *et al.* under the guidance of density functional theory calculations, found that SAs V has the best catalytic effect compared with SAs Fe, Mn, Ru, Zn, and Co. They successfully synthesized large-scale SACs V seeded on graphene to achieve high sulfur content (80 wt% sulfur), fast kinetic (a capacity of 645 mAh/g at 3 C rate) and long-life Li-S batteries. And the battery using S-SAV@NG as the cathode is very stable during the cycle, and the capacity decay is 0.073% per cycle at 0.5 C [55]. Therefore, in the future, applications and in-depth mechanistic analysis of SACs V and W in the cathode of Li-S batteries require further research.

5. Conclusion and prospectives

In summary, this review summarized the progress of research onto SACs for the cathodes of Li-S batteries. In catalytic reactions, SACs have several advantages including (i) an extraordinary catalytic activity and selectivity due to the unsaturated coordination sites of the active centers; (ii) strong bondings between SAs and supports on the interface facilitate charge transfer during electrochemical reactions; (iii) SACs ensure nearly 100% atomic utilization efficiency; and (iv) an improved understanding of catalytic reactivity mechanisms due to the presence of well-defined active sites [30,40,43]. In our discussion of recent publications, we found that using SACs on the positive electrode of Li-S batteries not only enhances the chemical interactions between the host surface and LiPSs, but also enhances the redox kinetics of LiPSs and minimizes the shuttle effect, which greatly improves the electrochemical performance of Li-S batteries. We summarized the strategies of synthesizing SACs in detail, including the spatial confinement and coordination design strategies. In the spatial confinement strategy, single atoms are confined to molecular-scale cages to avoid migration. Because of the space limitations of the microstructure, the uniform distribution of SACs is easy to realize. However, this strategy usually requires the formation of microstructures by pyrolysis at high temperatures, and the reaction conditions need to be strictly controlled, which limits the yield of a single atom. In the coordination design strategies, the coordination environment and local electron density state have a great influence on the catalytic performance. Moreover, the application of SACs in the cathodes of Li-S batteries, including iron, cobalt, and zinc, was intensively discussed. We can see that SACs can have a good catalytic effect, suitable for producing high-performance Li-S batteries. However, SACs also have some disadvantages, such as SAs are often susceptible to aggregation during preparation processes and the preparation of SACs is difficult and often requires a lot of energy [40]. Therefore, there are some key challenges in this area, so researchers have much work to complete in the future. The following topics need to be explored in greater depth.

(1) Increase the loading of the SACs. In most articles, the loading of the SACs is very low. Properly increasing the loading of SACs can fully catalyze the conversion of LiPSs and accelerate the electrochemical reaction. However, SACs tend to agglomerate when they are loaded onto the substrate materials because of their high surface energy. Therefore, it is very important to develop SACs which can be stabilized in the matrix, which would not only increase the loading of SACs but would also ensure that the active center of SACs is not lost, thus improving the overall catalytic performance. Balancing load and stability is still a challenge.
(2) Rational regulation of the local structure of SACs. Generally speaking, the catalytic effect of SACs is tightly associated with the coordination number and coordination sites of the surrounding atoms. Reasonable design of the local structure of the single atom can improve the affinity and catalytic performance of the LiPSs, but the accurate design of the local structure of the SACs still needs further effort.
(3) Designing new kinds of SACs. The SACs used in Li-S battery cathodes are mainly single Fe, Co, and Zn atoms. In order to widen the application of SACs in Li-S batteries, more kinds of SACs must be prepared. This would be more favorable for the application and development of SACs in Li-S batteries. In the synthesis of SACs, we should give full consideration to the coordination design strategy and spatial confinement strategy to ensure that more SACs were loaded and to make full use of the active centers of SACs.
(4) Further study of SACs. More research on the catalytic mechanism of SACs is needed. And more *in-situ* characterization and theoretical calculations are required to elucidate the catalytic mechanism of SACs. For example, XANES spectra and extended X-ray absorption fine structure (EXAFS) can be used to analyze the local electronic structure and chemical environment of the central atom at the atomic scale. Theoretical calculations such as reaction performance prediction, free Gibbs energy calculation, and so on could also be used to better study the catalytic process.

(5) A simple and low-cost method of synthesizing SACs needs to be found. Most of the synthesis methods of SACs used for the cathodes of Li-S batteries used pyrolysis. Although pyrolysis greatly improves the stability of single atoms, increases the SAs load, and improves the catalytic durability [43], the temperature of the pyrolysis method is above 600 °C [30], which requires high energy. We should focus on research into simpler synthesis methods to reduce the cost of synthesis and promote the development of SACs and their applications in other fields.

Declaration of competing interest

The authors declare that they have no known competing financial interests or personal relationships that could have appeared to influence the work reported in this paper.

Acknowledgments

This work was supported by the National Key Research and Development Program of China (No. 2020YFB1713500), the Student Research Training Plan of Henan University of Science and Technology (No. 2020026) and the National Undergraduate Innovation and Entrepreneurship Training Program (Nos. 202010464031, 202110464005).

References

[1] R. Wang, M. Mujahid, Y. Duan, et al., Adv. Funct. Mater. 29 (2019) 1808843.
[2] Y. Li, X. Zhai, Y. Liu, et al., Front. Mater. 7 (2020) 105.
[3] J. Chen, N.G. Park, Adv. Mater. 31 (2019) 1803019.
[4] Q. Zhao, X. Hao, S. Su, et al., J. Mater. Chem. A. 7 (2019) 15871–15879.
[5] Y. Sui, J. Zhou, X. Wang, et al., Mater. Today 42 (2021) 117–136.
[6] F. Tao, Y. Liu, X. Ren, et al., J. Energy Chem. 66 (2022) 397–412.
[7] F. Duffner, N. Kronemeyer, J. Tuebke, et al., Nat. Energy. 6 (2021) 123–134.
[8] B. Makuza, Q. Tian, X. Guo, et al., J. Power Sources 491 (2021) 229622.
[9] X. Hao, Q. Zhao, S. Su, et al., Adv. Energy Mater. 9 (2019) 1901604.
[10] Y. Wang, Z. Wang, D. Lei, et al., ACS Appl. Mater. Interfaces 10 (2018) 20244–20249.
[11] N. Liu, Z. Lu, J. Zhao, et al., Nat. Nanotechnol. 9 (2014) 187–192.
[12] M.K. Tran, M.T.F. Rodrigues, K. Kato, et al., Nat. Energy 4 (2019) 339–345.
[13] F. Wang, Y. Liu, H.J. Wei, et al., Rare Metals 40 (2021) 448–470.
[14] M. Cheviri, S. Lakshmipathi, Chem. Phys. Lett. 739 (2020) 136942.
[15] T. Ould Ely, D. Kamzabek, D. Chakraborty, et al., ACS Appl. Energy Mater. 1 (2018) 1783–1814.
[16] Y. Liu, H. Wei, X. Zhai, et al., Mater. Des. 211 (2021) 110171.
[17] G. Ye, M. Zhao, L.P. Hou, et al., J. Energy Chem. 66 (2022) 24–29.
[18] M. Zhao, X.Y. Li, X. Chen, et al., eScience 1 (2021) 44–52.
[19] P. Wang, B. Xi, Z. Zhang, et al., Angew. Chem. Int. Ed. 60 (2021) 15563–15571.
[20] L.L. Zhang, D.B. Liu, Z. Muhammad, et al., Adv. Mater. 31 (2019) 1903955.
[21] H. Zhao, B. Tian, C. Su, et al., ACS Appl. Mater. Interfaces 13 (2021) 7171–7177.
[22] X. Wang, C. Yang, X. Xiong, et al., Energy Storage Mater. 16 (2019) 344–353.
[23] H. Wei, J. Liu, Y. Liu, et al., Compos. Commun. 28 (2021) 100973.
[24] W. Yang, Y. Wei, Q. Chen, et al., J. Mater. Chem. A 8 (2020) 15816–15821.
[25] Z. Jin, M. Zhao, T. Lin, et al., J. Mater. Chem. A 8 (2020) 10885–10890.
[26] Z. Shen, Z. Zhang, M. Li, et al., ACS Nano 14 (2020) 6673–6682.
[27] R. Gan, N. Yang, Q. Dong, et al., J. Mater. Chem. A 8 (2020) 7253–7260.
[28] J. Jin, W. Cai, J. Cai, et al., J. Mater. Chem. A 8 (2020) 3027–3034.
[29] D. Liu, C. Zhang, G. Zhou, et al., Adv. Sci. 5 (2018) 1700270.
[30] Z. Zhang, J. Liu, A. Curcio, et al., Nano Energy 76 (2020) 105085.
[31] Q. Shao, L. Xu, D. Guo, et al., J. Mater. Chem. A 8 (2020) 23772–23783.
[32] Q. Wang, K. Ye, L. Xu, et al., Chem. Commun. 55 (2019) 14801–14804.
[33] W. Zang, Z. Kou, S.J. Pennycook, et al., Adv. Energy Mater. 10 (2020) 1903181.
[34] C. Wang, H. Song, C. Yu, et al., J. Mater. Chem. A 8 (2020) 3421–3430.
[35] J. Wang, L. Jia, H. Lin, et al., ChemSusChem 13 (2020) 3404–3411.
[36] Y. Chen, S. Ji, C. Chen, et al., Joule 2 (2018) 1242–1264.
[37] B. Singh, V. Sharma, R.P. Gaikwad, et al., Small 17 (2021) 2006473.
[38] Z. Liu, L. Zhou, Q. Ge, et al., ACS Appl. Mater. Interfaces 10 (2018) 19311–19317.
[39] Z. Du, X. Chen, W. Hu, et al., J. Am. Chem. Soc. 141 (2019) 3977–3985.
[40] F. Wang, J. Li, J. Zhao, et al., ACS Mater. Lett. 2 (2020) 1450–1463.
[41] R. Xiao, K. Chen, X. Zhang, et al., J. Energy Chem. 54 (2021) 452–466.
[42] Z. Zhuang, Q. Kang, D. Wang, et al., Nano Res. 13 (2020) 1856–1866.
[43] Y. Wang, F. Chu, J. Zeng, et al., ACS Nano 15 (2021) 210–239.
[44] Y. Wang, X. Huang, S. Zhang, et al., Small Methods 2 (2018) 1700345.
[45] K. Zhang, Z.X. Chen, R.Q. Ning, et al., ACS Appl. Mater. Interfaces 11 (2019) 25147–25154.
[46] H. Liu, X. Chen, X.B. Cheng, et al., Small Methods 3 (2019) 1800354.
[47] P. Wang, B. Xi, M. Huang, et al., Adv. Energy Mater. 11 (2021) 2002893.
[48] F. Tao, Y. Liu, X. Ren, et al., J. Alloys Compd. 873 (2021) 159742.
[49] J. Zheng, J. Tian, D. Wu, et al., Nano Lett. 14 (2014) 2345–2352.
[50] T.Z. Hou, X. Chen, H.J. Peng, et al., Small 12 (2016) 3283–3291.
[51] L. Zhang, P. Liang, H.B. Shu, et al., J. Colloid Interface Sci. 529 (2018) 426–431.
[52] T. Zhang, Z. Chen, J. Zhao, et al., Diamond Relat. Mater. 90 (2018) 72–78.
[53] H. Tian, A. Song, H. Tian, et al., Chem. Sci. 12 (2021) 7656–7676.
[54] E.I. Andritsos, C. Lekakou, Q. Cai, J. Phys. Chem. C 125 (2021) 18108–18118.
[55] G. Zhou, S. Wang, T. Wang, et al., Nano Lett. 20 (2020) 1252–1261.
[56] J. Wang, Z. Huang, W. Liu, et al., J. Am. Chem. Soc. 139 (2017) 17281–17284.
[57] J. Li, H. Huang, X. Cao, et al., Chem. Eng. J. 416 (2021) 127677.
[58] A. Wang, J. Li, T. Zhang, Nat. Rev. Chem. 2 (2018) 65–81.
[59] M. Yuan, X. Guo, Y. Liu, et al., J. Mater. Chem. A 7 (2019) 22123–22147.
[60] C. Lu, R. Fang, X. Chen, Adv. Mater. 32 (2020) 1906548.
[61] G. Liu, L. Xu, Y. Li, et al., Chem. Eng. J. 430 (2022) 132689.
[62] X.X. Wang, D.A. Cullen, Y.T. Pan, et al., Adv. Mater. 30 (2018) 1706758.
[63] Y. Li, J. Wu, B. Zhang, et al., Energy Storage Mater. 30 (2020) 250–259.
[64] L. Du, Q. Wu, L. Yang, et al., Nano Energy 57 (2019) 34–40.
[65] Q. Pang, X. Liang, C.Y. Kwok, et al., Nat. Energy 1 (2016) 16132.
[66] S. Zhang, S. Tsuzuki, K. Ueno, et al., Angew. Chem. Int. Ed. 54 (2015) 1302–1306.
[67] C. Lu, Y. Chen, Y. Yang, et al., Nano Lett. 20 (2020) 5522–5530.
[68] J. Wu, J. Chen, Y. Huang, et al., Sci. Bull. 64 (2019) 1875–1880.
[69] Y. Zhang, J. Liu, J. Wang, et al., Angew. Chem. Int. Ed. 60 (2021) 26622–26629.
[70] Y. Wang, D. Adekoya, J. Sun, et al., Adv. Funct. Mater. 29 (2019) 1807485.
[71] J. Wang, L.J. Jia, S.R. Duan, et al., Energy Storage Mater. 28 (2020) 375–382.
[72] X. Fan, S. Chen, W. Gong, et al., Energy Storage Mater. 41 (2021) 14–23.
[73] R. Wang, R. Wu, C. Ding, et al., Nano-Micro Lett. 13 (2021) 151.
[74] J. Ma, H. Wei, Y. Liu, et al., Int. J. Hydrogen Energy 45 (2020) 21205–21220.
[75] F. Wang, Y. Liu, Y. Zhao, et al., Appl. Sci. 8 (2018) 22.
[76] Y. Song, W. Zhao, L. Kong, et al., Energy Environ. Sci. 11 (2018) 2620–2630.
[77] G.S. Parkinson, Catal. Lett. 149 (2019) 1137–1146.
[78] Y. Li, G. Chen, J. Mou, et al., Energy Storage Mater. 28 (2020) 196–204.
[79] A. Phan, C.J. Doonan, F.J. Uribe-Romo, et al., Acc. Chem. Res. 43 (2010) 58–67.
[80] D. Zhang, S. Wang, R. Hu, et al., Adv. Funct. Mater. 30 (2020) 2002471.
[81] H. Shi, X. Ren, J. Lu, et al., Adv. Energy Mater. 10 (2020) 2002271.
[82] Z.Y. Han, S.Y. Zhao, J.W. Xiao, et al., Adv. Mater. 33 (2021) 2105947.
[83] D. Bresser, S. Passerini, B. Scrosati, Chem. Commun. 49 (2013) 10545–10562.
[84] X. Song, F. Zhou, M. Yao, et al., ACS Sustain. Chem. Eng. 8 (2020) 10185–10192.
[85] Y. Liu, Z. Wei, B. Zhong, et al., Energy Storage Mater. 35 (2021) 12–18.
[86] S. Zhang, X. Ao, J. Huang, et al., Nano Lett. 21 (2021) 9691–9698.
[87] J. Xie, B.Q. Li, H.J. Peng, et al., Adv. Mater. 31 (2019) 1903813.
[88] X. Meng, X. Liu, X. Fan, et al., Adv. Sci. 8 (2021) 2103773.
[89] Z.H. Zeng, W. Nong, Y. Li, et al., Adv. Sci. 8 (2021) 2102809.